IEEE Access
Multidisciplinary | Rapid Review | Open Access Journal

Received March 23, 2019, accepted April 4, 2019, date of publication May 8, 2019, date of current version June 5, 2019.

Digital Object Identifier 10.1109/ACCESS.2019.2915115

Online Dynamic Tip-Over Avoidance for a Wheeled Mobile Manipulator With an Improved Tip-Over Moment Stability Criterion

XIAOJUN DING[1,2], YI LIU[3], JIN HOU[1,2], AND QIN MA[3]

[1]School of Mechanical Science and Engineering, Huazhong University of Science and Technology, Wuhan 430074, China
[2]State Key Laboratory of Digital Manufacturing Equipment and Technology, Huazhong University of Science and Technology, Wuhan 430074, China
[3]School of Hydropower and Information Engineering, Huazhong University of Science and Technology, Wuhan 430074, China

Corresponding author: Yi Liu (prof_liuyi@hust.edu.cn)

This work was supported in part by the National Key R&D Program of China under Grant 2016YFC0402210, and in part by the Fundamental Research Funds for the Central Universities under Grant 2017KFYXJJ192.

ABSTRACT Tipping over avoidance is critical for the success of mobile manipulation, especially in the cases that the onboard manipulators or the mobile vehicles move rapidly. Due to strong dynamics coupling between the onboard manipulator and mobile vehicle, online evaluation of dynamic stability of mobile manipulators and generation of strategies for tip-over avoidance still remain challenging. This paper presents an improvement tip-over moment stability criterion dealing with wheel-terrain and vehicle-manipulator interaction and proposes a real-time tip-over avoidance algorithm to minimize the tip-over moment transfer through either adjusting the posture of the onboard manipulators or changing the running velocity of the vehicle. The simulations and experiments on a four-wheeled mobile manipulator validate the correctness and feasibility of the proposed method.

INDEX TERMS Mobile manipulator, tip-over avoidance, tip-over moment, wheeled–terrain interaction, vehicle–manipulator interaction.

I. INTRODUCTION

Mobile manipulator is an emerging class of robots which has capabilities of both moving and manipulation. A mobile manipulator is usually composed of a mobile vehicle with one or more onboard manipulators mounted on it, enabling it to be widely employed in manufacturing, logistics, home service, firefighting, dismantling bombs, disaster rescue, nuclear power stations, and even planetary exploration [1]–[4]. However, due to strong dynamics coupling between onboard manipulator(s) and mobile vehicle, a mobile manipulator inevitably tends to tip-over in the cases that it undergoes heavy load, moves at high velocity/acceleration, and/or negotiates rugged road. One of recent example is in the DARPA Robotics Challenge (DRC), where many robots failed due to tipping-over in the progress of the contest [5]. Therefore, tip-over avoidance is a prerequisite for a successful mobile manipulation.

Some tip-over stability criteria have been applied in mobile robots [7]–[12], and among them the Zero Moment Point (ZMP) method is the most popular. ZMP stability criterion has been applied for tip-over avoidance of a mobile manipulator by Huang *et al.* [7] and Sugano *et al.* [11]. , However, ZMP is not sensitive to the change in the center of mass (COM) [15] of the system, and it is unable to make a specific prediction for robot's instability [6], [13]. Then, Papadopoulos and Rey [14] reported the force-angle (FA) margin criterion, which can predict instability with a minimum angle between the resultant force exerted to the mobile platform and tip-over axis (TOA) normal. Although this criterion is sensitive to heavy loads, it requires the position COM must be known in advance and is only applied in a low velocity and large force condition. Moreover, this criteria also ignores reaction forces and moments where the manipulator exerts on the mobile platform, and then Moosavian and Alipour presented Moment-Height Stability (MHS) measure in consideration of robot's inertia about each axis of the support polygon [15]–[17]. MHS is sensitive to the whole system COM height. However, there is need to acquire the entire system COM position in advance, on account of its additional computation on the moment of inertia of the reference point of the moving vehicle coordinate system to each side [18],

The associate editor coordinating the review of this manuscript and approving it for publication was Zheng H. Zhu.

this criteria may be helpless for robot's real-time tip-over stability judgment. In addition, some other criteria are also employed in the stability detection of mobile manipulators, but there exist many different disadvantages. For example, normal supporting force criterion (NSF) [19] requests supporting forces can be measured with force sensors, which leads to a high cost. While there are plenty of complex computations in energy-equilibrium plane criterion (EEP) [20], which may cause the failure of real-time instability judgment [22], and effect of wheel-terrain interaction on robot's tip-over is not taken into account in tip-over moment (TOM) criterion [21]. Currently, many works have made specific presentations on tip-over stability for mobile manipulators in the process of climbing slopes or stairs. However, few pieces of literature published has reported a robot's tip-over stability resulting from the dynamic effect of its onboard manipulators and mobile platform.

Many tip-over avoidance algorithms have been proposed to avoid robots' tip-over in the motion process. For instance, Rey and Papadopoulos initialize manipulators' configuration to avoid robots' tip-over with FA measuring method [23]. Based on an adaptive neural fuzzy approach, Li and Liu utilize self-motions of redundant mobile manipulators to improve a robot's stability [24]. Alipour et al. have put forward a stability margin metric-increment function (SMMIF) and design relevant motion parameters with a fuzzy logic theory to prevent tip-over [25]. Liu et al. have reported a real-time tip-over avoidance algorithm, which makes the best of online change of tracked vehicle configuration and adjustment of onboard manipulator s' posture [19], [24]. Moreover, many other traditional algorithms (minimum distance method [26], adaptive control method [27], inverse motion method [28], genetic method [29] and neural network based on observer method Caron *et al.* [10]) have been being applied in robot's tip-over avoidance.

However, the research on the relationship between a low vehicle-manipulator mass ratio and tip-over stability of wheeled mobile manipulators remains challenging, especially in the motion process of high velocity. As is well-known, vehicle-manipulators interaction has an impact on robots with low vehicle-manipulator mass ratio: (1) In the low-velocity motion, the configuration of the onboard manipulator has great effects on the distribution of load, which may affect vehicle-terrain interaction; (2) In the motion with high acceleration, the velocity centroid of the systems may change, consequently taking impact on the vehicle-terrain interaction. In this paper, an improved tip-over moment stability criterion (ITOMSC) is proposed dealing with wheel-terrain interaction and vehicle-manipulator interaction. In contrast to exiting measures, this criterion has such advantages as great sensitivity to the COM, smaller computations cost, and better real-time performance and even there's no need to know the position of the entire system COM in advance. Meanwhile, a novel minimum amount of tip-over moment transfer based real-time tip-over avoidance algorithm is also presented with the help of the change of vehicle velocity and adjustment of onboard manipulator pose.

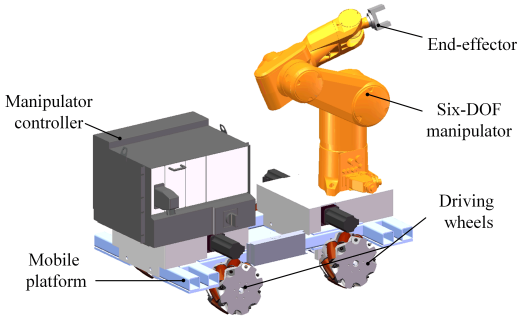

FIGURE 1. The CAD model of the wheeled mobile manipulator.

This paper is made up of six sections. Based on the kinematics and force model of this robot, wheel-terrain interaction and vehicle-manipulator interaction are analyzed in Section II. An improved ITOMSC criterion is presented in Section III. And then in Section IV, a novel real-time tip-over avoidance algorithm is proposed. In Section V, Simulation in MATLAB software and experiments are carried on in order to validate correctness of this improved tip-over stability criterion and the proposed real-time tip-over avoidance algorithm with this criterion, and in the final section, some conclusions on them are drawn.

II. KINEMATIC MODELING AND FORCE ANALYSIS OF WHEELED MOBILE MANIPULATOR

A. KINEMATIC MODEL OF THE WHEELED MOBILE MANIPULATOR

The wheeled mobile manipulator (WMM) under study consists of a four-wheel mobile platform, an end effector, a manipulator controller, and a manipulator mounted on the mobile platform, depicted in Fig. 1. The four-wheel mobile platform (called a vehicle for short) is composed of a chassis and four driving wheels which can be controlled to realize steering independently.

To describe the motion of the mobile manipulator, four coordinate systems are established, i.e., the world frame $O_WX_WY_WZ_W$, the ground frame $O_SX_SY_SZ_S$, the vehicle frame $O_MX_MY_MZ_M$,and the manipulator frame $O_RX_RY_RZ_R$, as shown in Fig. 2. In the frame $O_MX_MY_MZ_M$, the origin O_M is set as the projection of the vehicle center on the ground, in Fig. 2(a). Then, the motion of the vehicle on the ground can be determined by the position (d_{xm}, d_{ym}, d_{zm}), the yaw angle ϕ_m, and the pitch angle θ_m. Regarding the frame $O_RX_RY_RZ_R$, the origin O_R is selected to be the first joint frame of the onboard manipulator, which is confirmed by the centers of the vehicle-manipulator contacted area, O_RY_R and O_RZ_R are chosen to be parallel to O_MY_M and O_MZ_M, respectively, in Fig. 2(a). Then, the transformation matrices

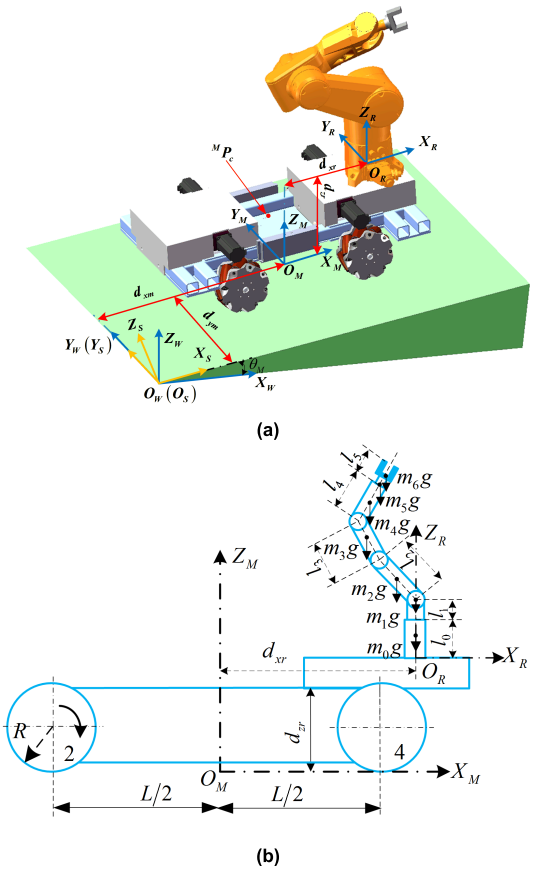

FIGURE 2. Coordinates system definition. (a) Coordinates system definition. (b) View along $O_M Y_M$.

between different frames are given as:

$$
{}^{W}_{S}\boldsymbol{T} = \begin{bmatrix} \cos\theta_m & 0 & -\sin\theta_m & 0 \\ 0 & 1 & 0 & 0 \\ \sin\theta_m & 0 & \cos\theta_m & 0 \\ 0 & 0 & 0 & 1 \end{bmatrix}
$$

$$
{}^{S}_{M}\boldsymbol{T} = \begin{bmatrix} \cos\phi_M & -\sin\phi_M & 0 & d_{xm} \\ \sin\phi_M & \cos\phi_M & 0 & d_{ym} \\ 0 & 0 & 1 & 0 \\ 0 & 0 & 0 & 1 \end{bmatrix}
$$

$$
{}^{M}_{R}\boldsymbol{T} = \begin{bmatrix} 1 & 0 & 0 & d_{xr} \\ 0 & 1 & 0 & 0 \\ 0 & 0 & 1 & d_{zr} \\ 0 & 0 & 0 & 1 \end{bmatrix} \tag{1}
$$

For the sake of simplification of analysis and computations conducted in the paper, the following assumptions are made:

1) the ground is even and no surface shrinkage is considered;

2) the center of gravity (COG) of the platform is coincided with its center of geometry;

3) all wheels are always in contact with the ground. i.e., no slippage of the wheels occurs;

4) the onboard manipulator is rigidly connected with the platform, and the links of the onboard manipulator are rigid.

The position-level kinematic equation of the mobile manipulator with respect to the frame $O_W X_W Y_W Z_W$ is derived following the DH method. The orientation of a generic link $i+1$ of the manipulator with respect to the link i is given by

$$
{}^{i}_{i+1}R = \begin{bmatrix} c\theta_{i+1} & -s\theta_{i+1} & 0 \\ s\theta_{i+1}c\alpha_i & c\theta_{i+1}c\alpha_i & -s\alpha_i \\ s\theta_{i+1}s\alpha_i & c\theta_{i+1}s\alpha_i & c\alpha_i \end{bmatrix} \tag{2}
$$

while the position of the link $i+1$ of the manipulator with respect to the link i, described with respect to the link i, is given by

$$
{}^{i}_{i+1}p = \begin{bmatrix} a_i \\ -s\alpha_i d_{i+1} \\ c\alpha_i d_{i+1} \end{bmatrix} \tag{3}
$$

A compact notation has been adopted for ${}^{i}_{i+1}R$ and ${}^{i}_{i+1}p$, where $c\theta_i := \cos\theta_i$ and $s\theta_i := \sin\theta_i$. So, the manipulator end effector position and orientation present in the manipulator frame $O_R X_R Y_R Z_R$ are

$$
{}^{0}_{i+1}p = \begin{cases} {}^{0}_{1}p, & i = 1 \\ {}^{0}_{i}p + \prod_{i=0}^{i-1} {}^{i}_{i+1}R\, {}^{i}_{i+1}p, & i > 1, i \subseteq Z \end{cases} \tag{4}
$$

$$
{}^{0}_{n+1}R = \prod_{i=0}^{n} {}^{i}_{i+1}R \tag{5}
$$

Based on the homogeneous coordinate transformation method, the position-level kinematic equation of the mobile manipulator with respect to the frame $O_W X_W Y_W Z_W$ is

$$
\begin{bmatrix} {}^{w}r_r & 1 \end{bmatrix}^T = {}^{W}_{S}T \cdot {}^{S}_{M}T \cdot {}^{M}_{R}T \cdot \begin{bmatrix} {}^{0}_{i+1}p & 1 \end{bmatrix}^T \tag{6}
$$

where ${}^{W}_{S}\boldsymbol{T}$, ${}^{S}_{M}\boldsymbol{T}$ and ${}^{M}_{R}\boldsymbol{T}$ can be obtained by Eq. (1). Here, take the first and second derivatives of Eq. (4) and (5), the recursive form expression of angular velocity, angular acceleration, linear velocity, linear acceleration, and linear acceleration at COM are obtained respectively, which are given as

$$
{}^{i+1}_{i+1}\boldsymbol{\omega} = {}^{i+1}_{i}\boldsymbol{R}\, {}^{i}_{i}\boldsymbol{\omega} + \dot{q}_{i+1} \cdot {}^{i+1}_{i+1}Z \tag{7}
$$

$$
{}^{i+1}_{i+1}\dot{\boldsymbol{\omega}} = {}^{i+1}_{i}\boldsymbol{R} \cdot {}^{i}_{i}\dot{\omega} + {}^{i+1}_{i}\boldsymbol{R} \cdot {}^{i}_{i}\boldsymbol{\omega} \times {}^{i+1}_{i+1}Z \cdot \dot{q}_{i+1} + \ddot{q}_{i+1} \cdot {}^{i+1}_{i+1}Z \tag{8}
$$

$$
{}^{i+1}_{i+1}\boldsymbol{v} = {}^{i+1}_{i}\boldsymbol{R}\left({}^{i}_{i}\boldsymbol{v} + {}^{i}_{i}\boldsymbol{\omega} \times {}^{i}_{i+1}\boldsymbol{p}\right) \tag{9}
$$

$$
{}^{i+1}_{i+1}\dot{\boldsymbol{v}} = {}^{i+1}_{i}\boldsymbol{R}\left({}^{i}_{i}\dot{\boldsymbol{v}} + {}^{i}_{i}\dot{\boldsymbol{\omega}} \times {}^{i}_{i+1}\boldsymbol{p} + {}^{i}_{i}\boldsymbol{\omega} \times \left({}^{i}_{i}\boldsymbol{\omega} \times {}^{i}_{i+1}\boldsymbol{p}\right)\right) \tag{10}
$$

$$
{}^{i+1}_{i+1}\dot{\boldsymbol{v}}_{\boldsymbol{c}} = {}^{i+1}_{i+1}\dot{\boldsymbol{v}} + {}^{i+1}_{i+1}\dot{\boldsymbol{\omega}} \times {}^{i+1}_{i+1}\boldsymbol{p}_{\boldsymbol{c}} + {}^{i+1}_{i+1}\boldsymbol{\omega} \times \left({}^{i+1}_{i+1}\boldsymbol{\omega} \times {}^{i+1}_{i+1}\boldsymbol{p}_{\boldsymbol{c}}\right) \tag{11}
$$

Meanwhile, it is easy to build the velocity-level kinematic equation of the vehicle, which is given in Eq. (12), as shown at the bottom of the next page. By using the principle of linear superposition, the velocity-level kinematic equation of the wheeled mobile manipulator is obtained, as shown in Eq. (13).

$$
{}^{w}\dot{\boldsymbol{r}}_{\boldsymbol{end}} = J\dot{\boldsymbol{q}} = {}^{r}\dot{\boldsymbol{r}}_{\boldsymbol{m}} + {}^{m}\dot{\boldsymbol{r}}_{\boldsymbol{w}} = \boldsymbol{J}_{\boldsymbol{r}}\dot{\boldsymbol{q}}_{\boldsymbol{r}} + \boldsymbol{J}_{\boldsymbol{m}}\dot{\boldsymbol{q}}_{\boldsymbol{m}} \tag{13}
$$

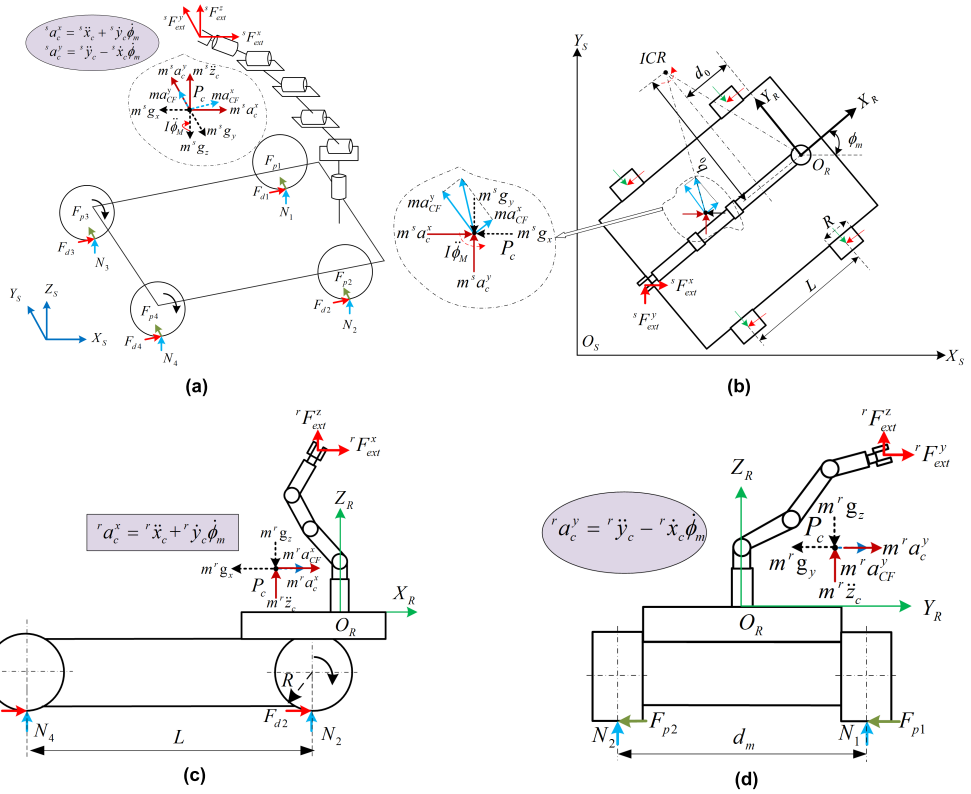

FIGURE 3. Force analysis for a wheeled mobile manipulator. (a) Simplified model. (b) View from the $O_S Z_S$ direction. (c) View along $O_M Y_M$. (d) View along $O_M X_M$.

where the Jacobi matrix of the onboard manipulator is calculated by Eq. (9).

B. FORCE MODEL OF THE WHEELED MOBILE MANIPULATOR

For simplification of representation, the masses of all parts of the mobile manipulator are simplified into the equivalent COG (see Fig. 3). Furthermore, for the convenience of calculations, the gravity acceleration vector $\boldsymbol{g} = \begin{bmatrix} 0 & 0 & -9.81 \end{bmatrix}^T$, the external force vector $\boldsymbol{f}_{ext} = \begin{bmatrix} F_{ext}^x & F_{ext}^y & F_{ext}^z \end{bmatrix}^T$, and the accelerations for the COG are projected to $O_S X_S Y_S Z_S$, $O_M X_M Y_M Z_M$ and $O_R X_R Y_R Z_R$ as follows [19]:

$$
\begin{aligned}
{}^s\boldsymbol{g} &= {}^W_S\boldsymbol{R}^T \cdot \boldsymbol{g} \quad {}^s\boldsymbol{f}_{ext} = {}^W_S\boldsymbol{R}^T \cdot \boldsymbol{f}_{ext} \\
{}^m\boldsymbol{g} &= {}^S_M\boldsymbol{R}^T \cdot {}^s\boldsymbol{g} \quad {}^m\boldsymbol{f}_{ext} = {}^S_M\boldsymbol{R}^T \cdot {}^s\boldsymbol{f}_{ext} \\
{}^r\boldsymbol{g} &= {}^M_R\boldsymbol{R}^T \cdot {}^m\boldsymbol{g} \quad {}^r\boldsymbol{f}_{ext} = {}^M_R\boldsymbol{R}^T \cdot {}^m\boldsymbol{f}_{ext} \\
\begin{bmatrix} {}^s\ddot{x}_c & {}^s\ddot{y}_c & {}^s\ddot{z}_c \end{bmatrix}^T &= {}^W_S\boldsymbol{R}^T \cdot \begin{bmatrix} {}^w\ddot{x}_c & {}^w\ddot{y}_c & {}^w\ddot{z}_c \end{bmatrix}^T \\
\begin{bmatrix} {}^m\ddot{x}_c & {}^m\ddot{y}_c & {}^m\ddot{z}_c \end{bmatrix}^T &= {}^S_M\boldsymbol{R}^T \cdot \begin{bmatrix} {}^s\ddot{x}_c & {}^s\ddot{y}_c & {}^s\ddot{z}_c \end{bmatrix}^T \\
\begin{bmatrix} {}^r\ddot{x}_c & {}^r\ddot{y}_c & {}^r\ddot{z}_c \end{bmatrix}^T &= {}^M_R\boldsymbol{R}^T \cdot \begin{bmatrix} {}^m\ddot{x}_c & {}^m\ddot{y}_c & {}^m\ddot{z}_c \end{bmatrix}^T
\end{aligned} \tag{14}
$$

where ${}^W_S\boldsymbol{R}$, ${}^S_M\boldsymbol{R}$ and ${}^M_R\boldsymbol{R}$ are rotation matrices, which can be obtained by Eq. (1). From Fig. 3(b), the x-direction and y-direction centrifugal accelerations can be determined as

$$
\begin{aligned}
a_{CF}^x &= \left({}^r x_c - d_0\right)\dot{\phi}_m^2 \\
a_{CF}^y &= \left(b_0 - {}^r y_c\right)\dot{\phi}_m^2
\end{aligned} \tag{15}
$$

where d_0 indicates the x-direction offset of the instant center of rotation (ICR) with respect to $O_R X_R Y_R Z_R$, which can be obtained from Fig. 3(b)

$$
d_0 = \begin{cases} 0, & \dot{\phi}_m = 0 \\ \dfrac{{}^s\dot{x}_r \sin\phi_m - {}^s\dot{y}_r \cos\phi_m}{\dot{\phi}_m}, & \dot{\phi}_m \neq 0 \end{cases} \tag{16}
$$

$$
{}^w\dot{\boldsymbol{r}}_r = \boldsymbol{J}_m\dot{\boldsymbol{q}}_m = \frac{\boldsymbol{R}}{4}\begin{bmatrix} 1-CB & 1+CB & 1-CB & 1+CB \\ -tan\alpha+CA & tan\alpha+CA & tan\alpha-CA & -tan\alpha-CA \\ C & -C & -C & C \end{bmatrix}\begin{bmatrix} \omega_1 \\ \omega_2 \\ \omega_3 \\ \omega_4 \end{bmatrix} \tag{12}
$$

where $A = \sqrt{d_{xr}^2 + d_{yr}^2} sin\alpha$, $B = \sqrt{d_{xr}^2 + d_{yr}^2} cos\alpha$, $C = \frac{1}{l+Lcot\alpha}$, $\alpha = arctan\frac{d_{yr}}{d_{xr}}$

where b_0 indicates they-direction offset of the ICR with respect to $O_RX_RY_RZ_R$, which can be writing as

$$b_0 = \begin{cases} 0, & \dot{\phi}_m = 0 \\ \dfrac{{}^s\dot{x}_r \cos\phi_m + {}^s\dot{y}_r \sin\phi_m}{\dot{\phi}_m}, & \dot{\phi}_m \neq 0. \end{cases} \tag{17}$$

The accelerations of the COG along O_RX_R and O_RY_R can be obtained from Fig. 3(c) and (d) as

$$\begin{aligned} {}^r a_c^x &= {}^r\ddot{x}_c - {}^r\dot{y}_c\dot{\phi}_m \\ {}^r a_c^y &= {}^r\ddot{y}_c + {}^r\dot{x}_c\dot{\phi}_m \end{aligned} \tag{18}$$

where the last item in Eq. (18) is the Coriolis acceleration. Moreover, wheel-terrain and vehicle-manipulator interactive force analysis is described as follows.

Each wheel is subjected to forces in three directions x, y, and z, i.e., tangential friction force F_{dj}, radial friction force F_{pj} and support force N_j(where j represent the number of the wheel) respectively. According to the vehicle dynamics [30], the force balance equation for WMM accelerated uphill can be derived by

$$\boldsymbol{F_t} = \boldsymbol{F_f} + \boldsymbol{F_w} + \boldsymbol{F_i} + \boldsymbol{F_a} \tag{19}$$

Namely,

$$\begin{bmatrix} F_{tx} \\ F_{ty} \end{bmatrix} = \begin{bmatrix} F_{fx} \\ F_{fy} \end{bmatrix} + \begin{bmatrix} F_{ax} \\ F_{ay} \end{bmatrix} + \begin{bmatrix} F_i \\ 0 \end{bmatrix} + \begin{bmatrix} F_{wx} \\ F_{wy} \end{bmatrix} \tag{20}$$

where $|\boldsymbol{F_t}| = \frac{\boldsymbol{P}\cdot\boldsymbol{i_r}\cdot\boldsymbol{\eta_T}}{\boldsymbol{nr}}$, $F_{tx} = |\boldsymbol{F_t}|\sin\beta$, $F_{ty} = |\boldsymbol{F_t}|\cos\beta$, $\boldsymbol{F_f} = \sum_{j=1}^{4} m_j g \begin{bmatrix} \mu_x & \mu_y \end{bmatrix}^T$, $F_i = m_m g sin\theta_m$, $F_{fx} = \sum_{j=1}^{4} F_{dj}$, $F_{fy} = \sum_{j=1}^{4} F_{pj}$, $F_{ax} = \sum_{j=1}^{4} m_j {}^s\ddot{x}_c$, $F_{ay} = \sum_{j=1}^{4} m_j {}^s\ddot{y}_c$.

C. INTERACTION OF WHEEL-TERRAIN AND VEHICLE-MANIPULATOR

1) WHEEL-TERRAIN INTERACTION

However, each wheel support force changes with the COG of the mobile manipulator. For the sake of simplicity, instead of analysis the force of each wheel independent, the overall effectiveness provided by the wheel-terrain contact is considered. Here, we ignored the influence of air resistance, so the acceleration provided to the vehicle by wheel-terrain interaction can be expressed as [30].

$$\begin{aligned} {}^s\ddot{\boldsymbol{x}}_{\boldsymbol{c}} &= \begin{bmatrix} {}^s\ddot{x}_c & {}^s\ddot{y}_c & {}^s\ddot{z}_c \end{bmatrix} \\ &= \begin{bmatrix} \dfrac{F_{tx} - F_{fx} - F_i}{m_m} & \dfrac{F_{ty} - F_{fy}}{m_m} & 0 \end{bmatrix} \end{aligned} \tag{21}$$

The vehicle can rotate around any axis at $\dot{\phi}_m$rad/s. From Fig. 3 (b), the accelerations of the COG along any axis in the frame $O_RX_RY_RZ_R$ can be obtained as

$$\begin{aligned} {}^s_r\boldsymbol{a_c} &= \begin{bmatrix} {}^s_r a_c^x \\ {}^s_r a_c^y \\ {}^s_r a_c^z \end{bmatrix} = \begin{bmatrix} {}_r a_c^x \\ {}_r a_c^y \\ {}_r a_c^z \end{bmatrix} + \begin{bmatrix} {}^r a_{CF}^x \\ {}^r a_{CF}^y \\ 0 \end{bmatrix} - \begin{bmatrix} {}^r g_x \\ {}^r g_y \\ {}^r g_z \end{bmatrix} \\ &= \begin{bmatrix} {}^r\ddot{x}_c - {}^r\dot{y}_c\dot{\phi}_m \\ {}^r\ddot{y}_c + {}^r\dot{x}_c\dot{\phi}_m \\ {}^r\ddot{z}_c \end{bmatrix} + \begin{bmatrix} a_{CF}^x \\ a_{CF}^y \\ 0 \end{bmatrix} - \begin{bmatrix} {}^r g_x \\ {}^r g_y \\ {}^r g_z \end{bmatrix} \end{aligned} \tag{22}$$

Meanwhile, the accelerations of the COG along any axis in the frame $O_MX_MY_MZ_M$ can be given as

$$\begin{aligned} {}^s_m\boldsymbol{a_c} &= \begin{bmatrix} {}^s_m a_c^x \\ {}^s_m a_c^y \\ {}^s_m a_c^z \end{bmatrix} = \begin{bmatrix} {}_m a_c^x \\ {}_m a_c^y \\ {}_m a_c^z \end{bmatrix} + \begin{bmatrix} {}^m a_{CF}^x \\ {}^m a_{CF}^y \\ 0 \end{bmatrix} - \begin{bmatrix} {}^m g_x \\ {}^m g_y \\ {}^m g_z \end{bmatrix} \\ &= \begin{bmatrix} {}^m\ddot{x}_c - {}^m\dot{y}_c\dot{\phi}_m \\ {}^m\ddot{y}_c + {}^m\dot{x}_c\dot{\phi}_m \\ {}^m\ddot{z}_c \end{bmatrix} + \begin{bmatrix} a_{CF}^x \\ a_{CF}^y \\ 0 \end{bmatrix} - \begin{bmatrix} {}^m g_x \\ {}^m g_y \\ {}^m g_z \end{bmatrix} \end{aligned} \tag{23}$$

2) VEHICLE-MANIPULATOR INTERACTION

In this paper, we utilize the relationship between the force and moment where the vehicle exerts on the onboard manipulator and the force and moment where the onboard manipulator 1-th joint exerts on the vehicle are mutual action and reaction. The Newton-Euler method [31] is employed to establish the dynamic equation of the onboard manipulator and solve the force and torque of the onboard manipulator exerts on the vehicle. Here we show the final results as

Mark $\boldsymbol{w}_i = \begin{bmatrix} {}^i_i\boldsymbol{f} \\ {}^i_i\boldsymbol{n} \end{bmatrix}$, we can obtain

$$\boldsymbol{w}_i = \boldsymbol{M}_i\boldsymbol{X}_i + \boldsymbol{H}_i + {}^i_{i+1}\boldsymbol{T}\cdot\boldsymbol{w}_{i+1} \tag{24}$$

where

$$\begin{aligned} \boldsymbol{M}_i &= \begin{bmatrix} m_i\boldsymbol{I}_3 & m_i {}^i_i\hat{\boldsymbol{p}}_{\boldsymbol{c}} \\ -m_i {}^i_i\hat{\boldsymbol{p}}_{\boldsymbol{c}} {}^i_i\hat{\boldsymbol{p}}_{\boldsymbol{c}} & {}^i_i\boldsymbol{I_c} \end{bmatrix} \\ \boldsymbol{X}_i &= \begin{bmatrix} {}^i_i\dot{\boldsymbol{v}}_{\boldsymbol{c}}\boldsymbol{\mathcal{C}}\boldsymbol{g} \\ {}^i_i\dot{\boldsymbol{\omega}} \end{bmatrix} \\ \boldsymbol{H}_i &= \begin{bmatrix} m_i \cdot {}^i_i\boldsymbol{\omega} \times \left({}^i_i\boldsymbol{\omega} \times {}^i_i\boldsymbol{p_c}\right) \\ -m_i \cdot {}^i_i\boldsymbol{\omega} \times \left({}^i_i\boldsymbol{\omega} \times {}^i_i\boldsymbol{p_c}\right) {}^i_i\hat{\boldsymbol{p}}_{\boldsymbol{c}} + {}^i_i\boldsymbol{\omega} \times {}^i_i\boldsymbol{I_c} \cdot {}^i_i\boldsymbol{\omega} \end{bmatrix} \\ {}^i_{i+1}\boldsymbol{T} &= \begin{bmatrix} {}^i_{i+1}\boldsymbol{R} & 0 \\ -{}^i_{i+1}\boldsymbol{R} {}^i_i\hat{\boldsymbol{p}}_{\boldsymbol{c}} & {}^i_{i+1}\boldsymbol{R} \end{bmatrix} \end{aligned} \tag{25}$$

where ${}^i_i\boldsymbol{\omega}$, ${}^i_i\dot{\boldsymbol{\omega}}$ and ${}^i_i\dot{\boldsymbol{v}}_{\boldsymbol{c}}$ can be obtained by Eq. (7), (8) and (11). Take the 6 DOFs (degree of freedom) manipulator (i.e. $i = 6$) as an example, and the force and moment numbered 7 is the force and moment acting on the endpoint of the onboard manipulator, i.e.

$$\boldsymbol{w}_7 = \begin{bmatrix} {}^7_7\boldsymbol{f} \\ {}^7_7\boldsymbol{n} \end{bmatrix} = \begin{bmatrix} {}^{tip}\boldsymbol{f} \\ {}^{tip}\boldsymbol{n} \end{bmatrix} = \begin{bmatrix} {}^{tip}\boldsymbol{f}_x & {}^{tip}\boldsymbol{f}_y & {}^{tip}\boldsymbol{f}_z & {}^{tip}\boldsymbol{n}_x & {}^{tip}\boldsymbol{n}_y & {}^{tip}\boldsymbol{n}_z \end{bmatrix} \tag{26}$$

which consists of two parts: the load gravity and inertia force and torque including the wrist mechanism and the force and torque subject to the environment.

From Eq. (17), $\boldsymbol{w}_1$can be obtained by this recursive computation till $i = 1$. The reaction wrench where the onboard manipulator act on the vehicle is expressed as $-\boldsymbol{w}_1$.

$$\boldsymbol{w}_1 = {}^i\boldsymbol{w}_1 + {}^v\boldsymbol{w}_1 + {}^{cf}\boldsymbol{w}_1 \tag{27}$$

where

$$
\begin{aligned}
{}^{i}\boldsymbol{w}_1 &= \boldsymbol{M}_1\boldsymbol{X}_1 + \boldsymbol{T}_{1,2}\boldsymbol{M}_2\boldsymbol{X}_2 + \ldots + \prod_{i=1}^{n}\boldsymbol{T}_{i-1,i}\boldsymbol{M}_n\boldsymbol{X}_n \\
&= \sum_{i=1}^{n}\boldsymbol{T}_{n-1,1}\boldsymbol{M}_n\boldsymbol{X}_n \\
{}^{v}\boldsymbol{w}_1 &= \boldsymbol{H}_1 + \boldsymbol{T}_{12}\boldsymbol{H}_2 + \boldsymbol{T}_{12}\boldsymbol{T}_{23}\boldsymbol{H}_2 + \ldots + \prod_{i=1}^{n}\boldsymbol{T}_{i-1,i}\boldsymbol{H}_2 \\
&= \sum_{i=1}^{n}\boldsymbol{T}_{n-1,1}\boldsymbol{H}_n \\
{}^{cf}\boldsymbol{w}_1 &= \prod_{i=1}^{n+1}\boldsymbol{T}_{i-1,i}\boldsymbol{w}_{n+1}
\end{aligned}
\tag{28}
$$

III. IMPROVED TIP-OVER MOMENT STABILITY MEASURE

In this section, we derive an ITOMSC for wheeled mobile manipulators with consideration of wheel-terrain and vehicle-manipulator interactions. Fig. 4 depicts the various forces and torques exerting on the mobile platform. The large ellipse represents the projection of the mobile platform on the ground. The force and torque exerted on the mobile platform consist of two parts, the force, and torque where the onboard manipulator exerted on the mobile platform and the force and torque generated by the wheel-terrain interaction. Based on the relationship between the force and torque ($\boldsymbol{F_R}$ and $\boldsymbol{M_R}$) where the onboard manipulator exerted on the mobile platform and the binding force and torque ($\boldsymbol{w_1}$) where the mobile platform exerted on the onboard manipulator 1-th joint, the former one adopts the Newton-Euler method.

$$
-\boldsymbol{w_1} = \begin{bmatrix}\boldsymbol{F_R} & \boldsymbol{M_R}\end{bmatrix}^T. \tag{29}
$$

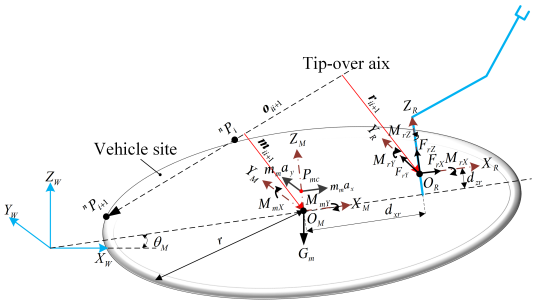

FIGURE 4. Forces and moments on a mobile platform.

While, for simplicity, the latter one provides acceleration $\boldsymbol{a_c}$ to the WMM, which provides traction in both the x and y directions. The influence of the acceleration generated by the wheel-terrain interaction on the onboard manipulator has been considered in the dynamic modeling, by setting the initial acceleration of the onboard manipulator 1-th joint, i.e. ${}^{0}_{0}\boldsymbol{a} = {}^{s}_{r}\boldsymbol{a_c}$. Where ${}^{s}_{r}\boldsymbol{a_c}$ can be calculated by Eq. (22). Therefore, only the influence of the acceleration generated by the wheel-terrain interaction on the vehicle is considered here. The acceleration is equivalent to the COM of the mobile platform (P_{mc}),i.e. $\begin{bmatrix}a_x & a_y & 0\end{bmatrix} = \begin{bmatrix}{}^{s}_{m}a^x_c & {}^{s}_{m}a^x_c & 0\end{bmatrix}$, as shown in Fig. 4, where ${}^{s}_{m}a^x_c$ and ${}^{s}_{m}a^y_c$ can be obtained by Eq. (23).

Considering all the forces and moments mentioned above, the TOM on the TOA $\boldsymbol{o}_{ii+1}$ can be calculated as

$$
\begin{aligned}
\boldsymbol{TOM}_{ii+1} = \boldsymbol{M_R}\cdot\boldsymbol{o}_{ii+1} + (\boldsymbol{r}_{ii+1}\times\boldsymbol{F_{rZ}})\cdot\boldsymbol{o}_{ii+1} + \boldsymbol{M_M}\cdot\boldsymbol{o}_{ii+1} \\
+ (\boldsymbol{m}_{ii+1}\times\boldsymbol{G_M})\cdot\boldsymbol{o}_{ii+1}
\end{aligned}
\tag{30}
$$

the first item in the right of Eq. (30) is the projection of the moment where the onboard manipulator exerted on the mobile platform on the TOA. The second item is the moment of the force component in the Z_R direction where the onboard manipulator exerted on the mobile platform on the TOA. The third item is the projection of the moment where the ground exerted on the mobile platform on the TOA. The last item is the moment of the force component in the Z_M direction where the ground exerted on the mobile platform on the TOA.

If tipping occurs, the robot will tip over along the TOA formed by two adjacent wheels. Where $\boldsymbol{o}_{ii+1}$ represents a unit vector for the TOA, which can be obtained by the coordinates of two adjacent wheel-terrain contact points $({}^{n}\boldsymbol{p}_i, {}^{n}\boldsymbol{p}_{i+1})$, i.e.

$$
\boldsymbol{o}_{ii+1} = ({}^{n}\boldsymbol{p}_{i+1} - {}^{n}\boldsymbol{p}_i)/|{}^{n}\boldsymbol{p}_{i+1} - {}^{n}\boldsymbol{p}_i| \tag{31}
$$

$\boldsymbol{r}_{ii+1}$ represents an orthogonal vector from point O_R to the TOA $\boldsymbol{o}_{ii+1}$. $\boldsymbol{m}_{ii+1}$ represents an orthogonal vector from point O_M to the TOA $\boldsymbol{o}_{ii+1}$. According to the dynamic method of the rigid body translation, the moments of the onboard manipulator and the mobile platform relative to the TOA ${}^{n}\boldsymbol{p}_i{}^{n}\boldsymbol{p}_{i+1}$ on the corresponding coordinate system is calculated respectively. When the mobile platform performs the acceleration or deceleration, the force and torque where the onboard manipulator exerted on the mobile platform are

$$
\begin{aligned}
\boldsymbol{F_R} &= \begin{bmatrix}F_{rX} & F_{rY} & F_{rZ}\end{bmatrix}^T \\
&= -\begin{bmatrix}{}^{1}F_X & {}^{1}F_Y & {}^{1}F_Z\end{bmatrix}^T \\
\boldsymbol{M_R} &= \begin{bmatrix}M_{rX} - F_{rY}\cdot d_{zr} & M_{rY} + F_{rX}\cdot d_{zr} & M_{rZ}\end{bmatrix}^T
\end{aligned}
\tag{32}
$$

similarly, the force and torque generated by the wheel-terrain interaction on the mobile platform can be written as

$$
\begin{aligned}
\boldsymbol{F_M} &= \begin{bmatrix}F_{mX} & F_{mY} & F_{mY}\end{bmatrix}^T \\
&= \begin{bmatrix}m_M{}^{m}a^y_c - G_M sin\theta & m_M{}^{m}a^x_c & G_M cos\theta\end{bmatrix}^T \\
\boldsymbol{M_M} &= \begin{bmatrix}m_M{}^{m}a^y_c\cdot{}^{m}Z_{mc} & \left(m_M{}^{m}a^x_c - G_M sin\theta\right)\cdot{}^{m}Z_{mc} & 0\end{bmatrix}^T.
\end{aligned}
\tag{33}
$$

The contact points of the mobile platform and the ground are sequentially connected in a counterclockwise direction to form a polygonal convex hull. If the side length of the convex hull regarded as the rotation axis, the overturning moment can be obtained. By comparing the magnitude of the overturning moment of each of the tilting axes, the maximum overturning moment TOM_{max} is obtained. TOM_{max} represents the maximum overturning moment sustained by the system on the tilting axis corresponding to the value. If the value of TOM_{max}

is positive, the system is tipping over. While, if negative, the system is stable with a TOM margin $|TOM|$.

This criterion may significantly differ from ZMP, FA, and MHS. ZMP obtains the point where the reaction force acts on the ground, thus obtaining the boundary where the force cannot cross, making the system stable. FA uses the angle between the resultant force which exerting on the ground COM and a particular vector to describe the system's stability. MHS estimates the stability of the system by calculating the inertia of the robot on each axis of the supporting polygon. These measurement methods evaluate the stability with an indicator [32], while in ITOMSC the moment is used to describe the stability. The criterion is sensitive to the TOM, easy-to-compute, easy-implementing and suitable for wheeled robot systems that are running on any terrain and subjected to centrifugal force, inertial force and other external forces.

IV. ONLINE TIP-OVER AVOIDANCE ALGORITHM

We predict the tip-over stability of the mobile manipulator by using ITOMSC, i.e., when $|TOM_{max}| \to 0$ with $t \to T$ (T represents a period of time), the wheel at these points can be off the ground, and tipping instability can also occur. Here, zero supporting forces are considered to be the critical tip-over stable state. In this case, the robot may topple down subject to a small disturbance force. So, the TOM_{max} should be negative enough. If $TOM_{max} << 0$ with $t \to T$, the system will be more stable. For simplification of tip-over avoidance, the Eq. (23) can be rewritten as

$$\boldsymbol{TOM}_{ii+1} = \boldsymbol{TOM}_{opt} + \Delta\boldsymbol{TOM}_{ii+1} \tag{34}$$

where $\Delta\boldsymbol{TOM}_{ii+1} = \left[\Delta TOM^x_{ii+1}\ \Delta TOM^y_{ii+1}\ \Delta TOM^z_{ii+1}\right]$, $\boldsymbol{TOM}_{opt}$ is a moment in the robot optimal configuration which the values of TOM on all tip-over axes are similar. ΔTOM^x_{ii+1}, ΔTOM^y_{ii+1} and ΔTOM^z_{ii+1} represent the change of TOM caused by TOM transfer due to the COG offset, the centrifugal forces, the inertial forces, as well as the external forces.

From the above analysis of tip-over stability, it is hard to get an explicit expression for the TOM at the selected TOA. Here, an online tip-over avoidance algorithm is proposed by minimizing the TOM transfer to balance the TOM distribution on each TOA. As the most stable situation corresponds to even TOM distribution on all the tip-over axes, i.e., without any TOM transfers. Therefore, the robot should be adjusted to meet $\boldsymbol{TOM}_{ii+1} \to \boldsymbol{TOM}_{opt}$, that is $\Delta TOM^x_{ii+1} + \Delta TOM^y_{ii+1} + \Delta TOM^z_{ii+1} \to 0$ as $t \to \infty$. Furthermore, the tip-over avoidance optimization function can be obtained as

$$\sigma = \sum_{i=1}^{n} \frac{1}{2} \|\Delta TOM_{ii+1}\|_2^2 \tag{35}$$

To improve the tip-over stability of the wheeled mobile manipulator, the pose of the onboard manipulator can be regulated to balance the TOM distribution. Also, the velocity of the wheeled mobile platform can change to balance the TOM distribution either. Therefore, an online tip-over avoidance algorithm can be defined by

$$\begin{aligned} \dot{q}_i &= -k_i \frac{\partial \sigma}{\partial q_i} \\ \dot{\xi} &= -k_m \frac{\partial \sigma}{\partial \xi} \end{aligned} \tag{36}$$

where $k_i > 0$, $k_m = \left[k_x\ k_y\ k_z\right]$, $k_x > 0$, $k_y > 0$, $k_z > 0$ are constants, $\theta_i \in [0, 2\pi]$, and the physical limits should not be surpassed, i.e., $q_i \in (q_{i\min}, q_{i\max})$, $\dot{q}_i \in (\dot{q}_{i\min}, \dot{q}_{i\max})$, $\dot{\xi} = \left[{}^m\dot{x}_m\ {}^m\dot{y}_m\ {}^m\dot{\phi}_m\right]^T$, $\dot{\xi} \in \left(\dot{\xi}_{\min}, \dot{\xi}_{\max}\right)$.

Algorithm 1 Tip-Over Prediction and Avoidance

Input: $\theta_m, m_m, m_r, d_{zr}, {}^mZ_{mc}, \mathbf{a}, TOM_1, TOM_2, q^i_{now}, \dot{q}^i_{now}, \ddot{q}^i_{now}(i = 1\ldots6), \dot{\xi}_{now}$
Output: $\dot{q}^i_{next}(i = 1\ldots6), \dot{\xi}_{next}$

While not The task complete
  if Tip-over detection cycle arrival
    if The ground can provide enough tractive force
      Calculating $F_{rZ}, M_{rX}, M_{rY}, \mathbf{a}$ and G_M
      Calculate the TOM and the TOM_{max}
      if $max\{TOM\} \leqq TOM_1$
        if $\{TOM\} \geqq TOM_2$
          Calculating the optimization function

$$\sigma = \frac{1}{2} \sum_{i=1}^{n} \|\Delta TOM_{ii+1}\|$$

          if The manipulator in the optimal configuration
            Changing the wheeled mobile platform's velocity by

$$\dot{\xi} = -k_m \frac{\partial \sigma}{\partial \xi}$$

          else Adjusting the onboard Manipulator according to

$$\dot{q}_i = -k_i \frac{\partial \sigma}{\partial q_i}$$

          end if
        else Continue the task
        end if
      else Reporting error, sending stop request and exit
      end if
    else Reporting error, sending stop request and exit
    end if
  else Continue the task
  end if
end while

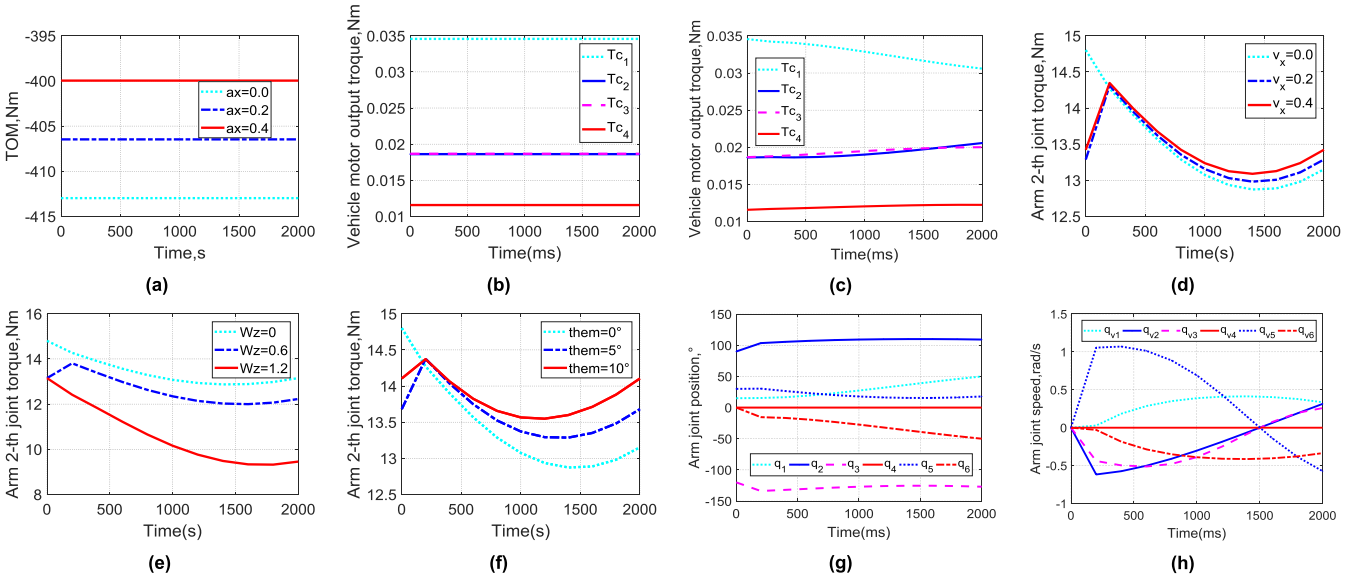

FIGURE 5. Interaction analysis. (a) TOM of the TOA12, case 1, scheme 1. (b) The vehicle output drive torque, case 2, scheme 1. (c) The vehicle output drive torque, case 2, scheme 2. (d) The manipulator 2-th joint torque, case 2, scheme 1. (e) The manipulator 2-th joint torque, case 2, scheme 1. (f) The manipulator 2-th joint torque, case 2, scheme 1. (g) Joint angles, case 2, scheme 2. (h) Joint angular velocities, case 2, scheme 2.

The tip-over avoidance algorithm described in Eq. (36) and (36) should be triggered when necessary. In addition, the robot movement must be stopped under the situation which the pose of onboard manipulator adjustment or the vehicle velocity change is not enough to restore the rollover stability. Furthermore, if tip-over stability can be restored by regulating the onboard manipulator, the velocity of the wheeled mobile platform should not be changed to maintain good traction. Thus, an online tip-over prediction and avoidance algorithm is proposed, given in Algorithm 1. In applications, the robot may be affected by measurement errors and uncertainty disturbances. Therefore, in order to make sure that the robot is terminated before overturn and the algorithm is triggered when necessary, margins (TOM_1 and TOM_2) should be added to the ITOMSC respectively.

TABLE 1. Design parameters for the robot.

Parameters	Values	Parameters	Values
$L(\mathrm{mm})$	510.00	$m_m(\mathrm{kg})$	153.80
$d_m(\mathrm{mm})$	475.00	$m_r(\mathrm{kg})$	51.00
$d_{xm}(\mathrm{mm})$	200.00	$m_0(\mathrm{kg})$	10.44
$d_{ym}(\mathrm{mm})$	200.00	$m_1(\mathrm{kg})$	15.66
$d_{xr}(\mathrm{mm})$	385.00	$m_2(\mathrm{kg})$	9.61
$d_{zr}(\mathrm{mm})$	303.84	$m_3(\mathrm{kg})$	10.14
${}^mZ_{mc}(\mathrm{mm})$	235.00	$m_4(\mathrm{kg})$	4.85
$TOM_1(\mathrm{Nm})$	-10.00	$m_5(\mathrm{kg})$	0.16
$TOM_2(\mathrm{Nm})$	-600.00	$m_6(\mathrm{kg})$	0.08
$R(\mathrm{mm})$	101.60		

V. SIMULATION AND EXPERIMENTALS

A. SIMULATION SETUP AND RESULTS

1) SIMULATION SETUP

In order to verify the correctness and feasibility of the presented wheel-terrain and vehicle-manipulator interaction analysis method and the proposed tip-over avoidance algorithm, simulations have been carried out on a WMM, which is consisted of a 6-DOF onboard manipulator and a four-wheeled vehicle, as shown in Fig.1. The robot's design parameters are shown in Table 1. Simulations were conducted for four different cases which the time interval is set to be $t \in [0, 2]$ s, the incline angle of the ground θ_m is set to be equal to zero, and a 1-kg payload is selected to the end-effector.

Case 1 is used to verify wheel-terrain interaction. The vehicle is controlled to follow a straight line, which is determined by ${}^m\dot{x}_m = 0.04\lambda t$, with different acceleration by changing λ. The feedback velocity of the vehicle with respect to the frame $O_W X_W Y_W Z_W$ can be calculated by Eq. (12). The onboard manipulator is in the initial configuration which is $q_0 = \begin{bmatrix} \pi/12 & \pi/2 & -2\pi/3 & 0 & \pi/6 & 0 \end{bmatrix}^T$.

Case 2 is used to verify the vehicle-manipulator interaction. The vehicle is controlled to follow a straight line, which is determined by ${}^m\dot{x}_m = 0.1$. The onboard manipulator is controlled to follow a circle, which is described by ${}^r x_r = 0.1 + 0.05\sin(\pi t/2)$, ${}^r y_r = 0.1 - 0.05\cos(t/2)$ and ${}^r z_r = 0.27$. The end feedback position of the onboard manipulator with respect to the frame $O_W X_W Y_W Z_W$ can be obtained by Eq. (6), the end feedback velocity of the onboard manipulator with respect to the frame $O_W X_W Y_W Z_W$ can be gained by Eq. (13). Besides, the incline angle of the ground θ_m is set to be 5° to demonstrate the vehicle-manipulator interactions when negotiating slope.

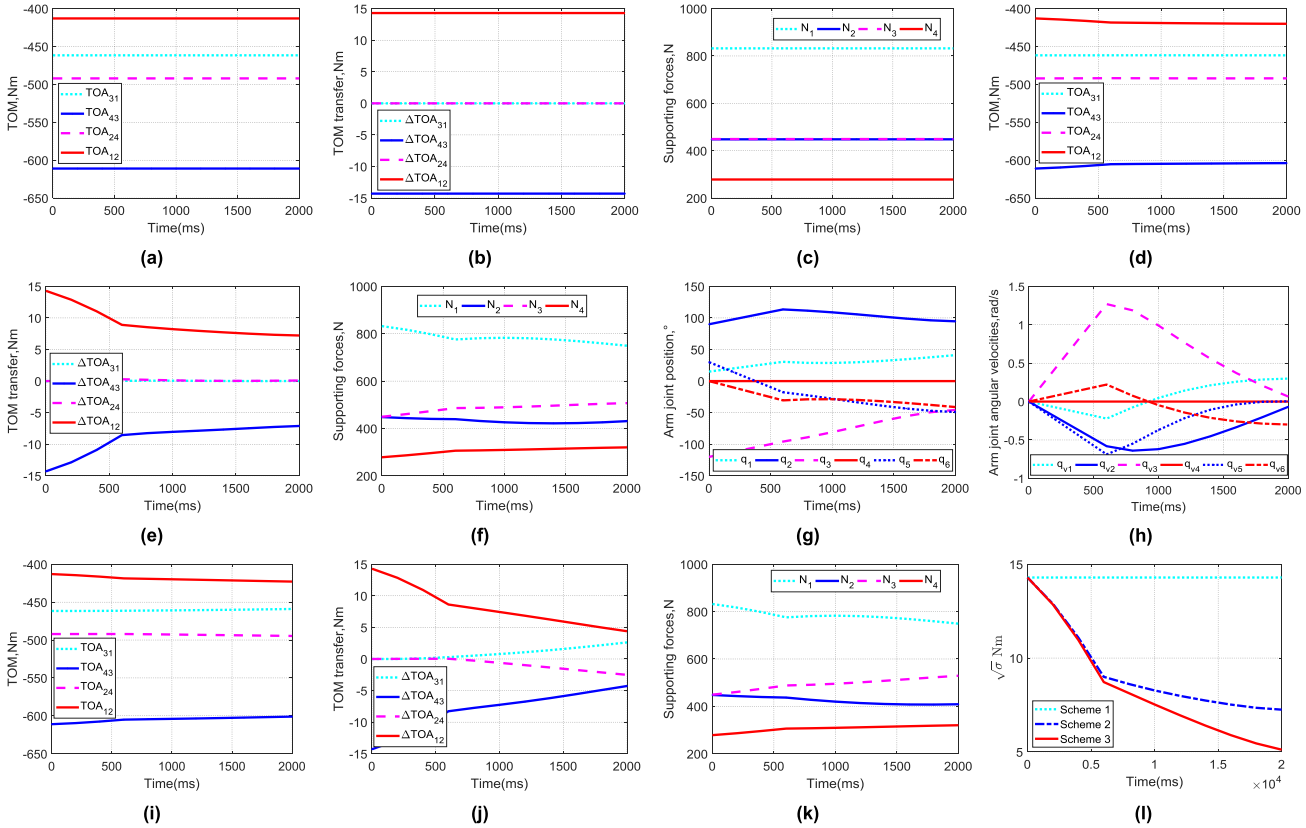

FIGURE 6. Simulation results. (a) TOM, case 3, scheme 1. (b) TOM transfer, case 3, scheme 1. (c) Supporting force, case 3, scheme 1. (d) TOM, case 3, scheme 2. (e) TOM transfer, case 3, scheme 2. (f) Supporting force, case 3, scheme 2. (g) Joint angles, case 3, scheme 2. (h) Joint angular velocities, case 3, scheme 2. (i) TOM, case 4, scheme 3. (j) TOM transfer, case 4, scheme 3. (k) Supporting force, case 4, scheme 3. (l) The square root of σ, case 3,4, scheme 1-3.

Case 3 is used to test the tip-over avoidance algorithm by adjusting the onboard manipulator. The vehicle is controlled to follow a straight line, which is determined by ${}^{m}\dot{x}_m = 0.1$, and the onboard manipulator is adjusted by the tip-over avoidance algorithm obtained in Eq. (36).

Case 4 is used to test the tip-over avoidance algorithm by changing the velocity of the vehicle. Under the condition of case 3, the vehicle velocity $\dot{\xi}$ is changed by the tip-over avoidance algorithm given by Eq. (36).

Simulations are made for three different schemes for each case: in scheme 1, the onboard manipulator remained in the initial configuration. In scheme 2, the onboard manipulator is adjusted by the tip-over avoidance algorithm given in Eq. (36). In scheme 3, the velocity of the vehicle is changed according to the tip-over avoidance algorithm given in Eq. (36). The joint limits are set to be $q_1 \in [-\pi, \pi]$ and $q_i \in [-2/3\pi, +2/3\pi]\,(i = 2, 3, \ldots, 6)$. Moreover, the limit of each joint angular velocity is set to be $\dot{q}_i \in [-2, +2]\,rad/s$. The limit of the vehicle velocity is set to be $\dot{\xi} \in \left(\left[-0.4\ -0.4\ -0.8\right]^T, \left[0.4\ 0.4\ 0.8\right]^T\right)$ m/s,rad/s. Furthermore, the coefficient of rolling friction is selected to be $\mu_x = \mu_y = 0.02$. The constants in scheme 2 are selected as $k_i = 1 \times 10^{-4}\,(i = 1, 2 \ldots, 6)$ the constants in scheme 3 are selected as $k_m = \left[0.2\ 0.2\ 0.6\right]$.

2) SIMULATION RESULTS AND DISCUSSION

Simulation results for the wheel-terrain and the vehicle-manipulator interactions are presented in Fig.5. Once the terrain is determined, the wheel-terrain interaction provides different traction forces for the vehicle, which is the different accelerations, will affect the TOM.

Fig. 5(a) shows the change of the TOM of the TOA_{12} under different accelerations. The TOM increases with the increase of the acceleration, and the WMM tends to be unstable. Compared with literature [21], the wheel-terrain interaction cannot be ignored because the TOM values vary from -413 to -406 when λ increases from 0 to 0.2. As shown in table 2, variables n and N represent the number of support polygon vertices and DOF of the onboard manipulator in the measuring as mentioned above methods respectively. Then, when $n = 4$ and $N = 6$ in such system depicted in Fig. 1, it can indicate that ITOMSC algorithm shows better timeliness. Furthermore, comparing Fig. 5(c) with (b), the vehicle motor output torque is affected according to the vehicle-manipulator interactions, which are caused by the movement of the onboard manipulator, as shown in Fig. 5(g) and (h). This reveals the effect of the onboard manipulator on the vehicle during vehicle-manipulator interactions. Fig. 5(d) and (e) demonstrate how the onboard manipulator joint drive torque

TABLE 2. The computational complexity of different measures [17].

Dynamic Stability Measure	Multiplications	Additions
Energy based	$91n$	$54n$
Force-Angle	$76n$+4	$52n$+2
MHS	$17n$+$35N$+13	$13n$+$24N$+5
ITOM	$18n$	$12n$+3

TABLE 3. Performance evaluation for simulation results.

Case	Scheme	$\Delta\lvert\text{TOM}\rvert_{\max}$	$\text{TOM}_{\max}$	$\sqrt{\frac{\sum_{i=1}^{N}\sigma(t_i)}{N_t}}$	Stable?
3	1	14.29	-412.98	14.29	yes
3	2	7.22	-420.05	9.55	yes
4	3	4.39	-422.88	8.88	yes

(taking the second joint as an example) are affected according to the vehicle-manipulator interactions, which are caused by the vehicle velocity change (linear velocity v_x or angular velocity w_z). Also, it is affected by the change of the incline angle to the ground θ_m, which is shown in Fig. 5(f). While the torque T_2 increases with v_x and decreases with w_z or θ_m. This illustrated the effect of the vehicle on the onboard manipulator during vehicle-manipulator interactions. The joint angles and joint angular velocities of the onboard manipulator in the motion process are shown in Fig. 5(g) and (h).

The simulation results for the tip-over avoidance algorithm with adjusting the pose of the onboard manipulator or change the vehicle velocity are presented in Fig. 6. Fig. 6 (a), (d) and (i) represent the TOM for the three different schemes with four different TOA. Fig.6(b), (e) and (j) represent the TOM transfers for three different schemes with four different TOA. Supporting forces are illustrated in Fig. 6 (c), (f) and (k), respectively. Comparing Fig. 6(c) with (f), it can be seen that the supporting forces of the four wheels become closer, i.e., the stability is improved. The phenomenon can also be seen from TOM or TOM transfers either. The joint angles and joint angular velocities of the onboard manipulator in the motion process in scheme 2 are shown in Fig. 6(g) and (h). The square root of the optimization function, i.e., $\sqrt{\sigma}$ (The smaller the value, the more stable the system is), which represents TOM transfers, is compared with the three different schemes, as shown in Fig. 6(l). It shows that stability can be improved by adjusting the pose of the onboard manipulator. Moreover, owing to changing its velocity while adjusting the onboard manipulator, the vehicle can show better stability.

The maximum TOM, the maximum TOM transfer, and the robot tip-over stability are compared in Table 3 for three different schemes with two different cases. N_t denotes the sampling numbers and $\sigma\ (t_i)$ represents the optimization function at the time instant t_i. From Table 3, it can be observed that the TOM_{max}, the $\Delta|TOM_{max}|$ and the $\sqrt{\sigma}$ are obviously reduced

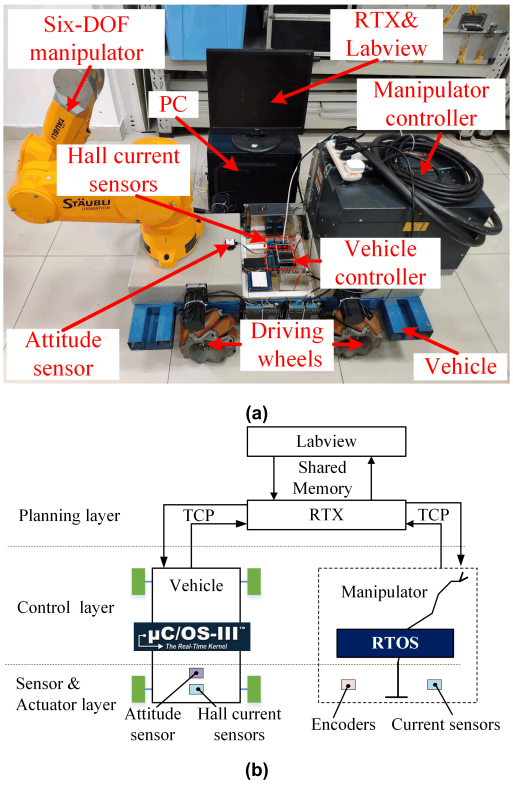

FIGURE 7. (a) Photo and (b) control system composition.

by comparing three different schemes. From Fig. 8(a)-(l) and Table 3, the proposed tip-over avoidance algorithm can effectively to balance the TOM distribution, and the stability of the robot has been obviously improved.

The simulation results for case 1 and case 2 demonstrate that the robot may keep stable without optimum configuration, i.e. the tip-over avoidance algorithm should be triggered when necessary. Furthermore, the simulation results of case 3 and case 4 give an example of applying the algorithm to avoid tip-overs.

B. EXPERIMENTAL RESULTS

1) EXPERIMENTAL SETUP FOR THE WMM

The experimental photo and the composition of control system are shown in Fig. 7. An attitude sensor (model BWT901CL) was employed to measure the rolling angle of the body which mounted on the vehicle body. The hall current sensors (model HBC-LSP-6) were used to measure the driving current of the vehicle wheels. The vehicle controlled by a microprocessor (model STM32F407ZGT6) with μc/os III operating system. The manipulator (model Staubli TX60) controlled by a real-time operating system (RTOS). In addition, RTX3.0 was used to build an RTOS on Windows, which establish a real-time Ethernet (at a planning cycle of 1 ms) using TCP protocols between the planning layer and the control layer. LabVIEW was used to realize human-computer

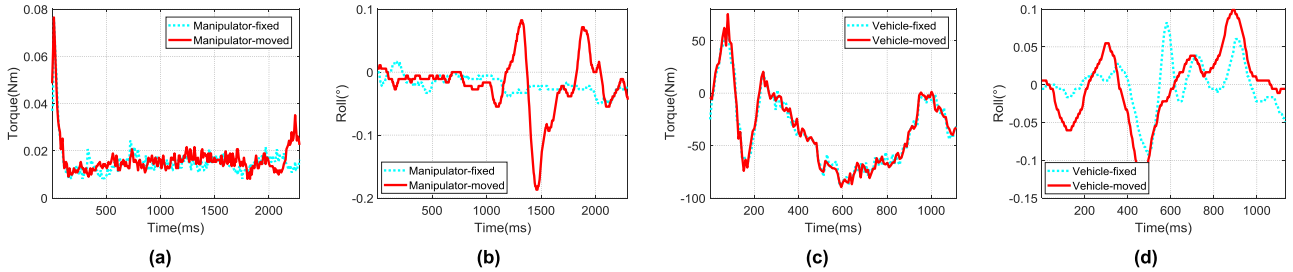

FIGURE 8. Interaction analysis. (a) The vehicle's first wheel output torque. (b) The vehicle body rolling angle (vehicle fixed). (c) The manipulator's second joint driving torque. (d) The vehicle body rolling angle (manipulator fixed).

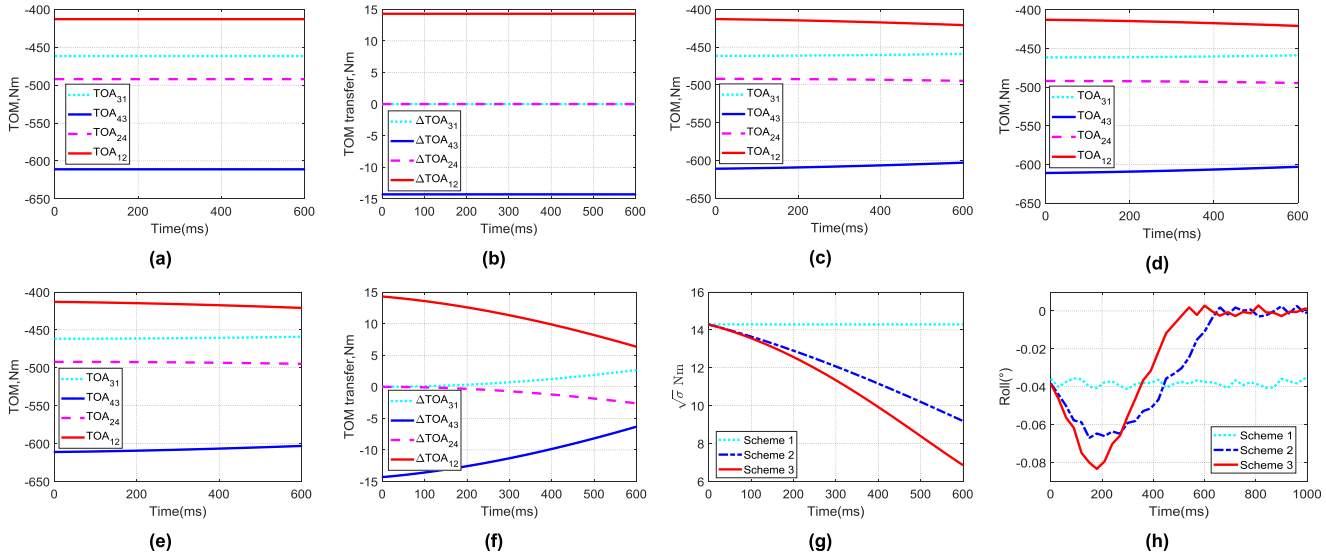

FIGURE 9. Experiment results. (a) TOM, scheme 1. (b) TOM transfer, scheme 1. (c) TOM, scheme 2. (d) TOM transfer, scheme 2. (e) TOM, scheme 3. (f) TOM transfer, scheme 3. (g) The square root of σ, scheme 1-3. (h) The vehicle body rolling angle, scheme 1-3.

interaction, which exchanged data with RTX through shared memory.

2) EXPERIMENTAL RESULTS AND DISCUSSION

In this section, and the proposed tip-over avoidance algorithm by the presented tip-over prediction criterion will be demonstrated through experiments on a WMM, as shown in Fig. 7(a). The first experiment is designed to verify the wheel-terrain and vehicle-manipulator interactions, and the second experiment is designed to confirm the effectiveness of the proposed tip-over avoidance algorithm by the presented tip-over prediction criterion.

Figure 8(a) and (b) show the influence of the interaction between the onboard manipulator and the vehicle on the vehicle, which is represented by the output torque of the vehicle (taking the first wheel as an example) and the rolling angle of its body (vehicle fixed). We can see that the amplitude of the output torque is suddenly changed with the movement of the onboard manipulator at the time close to 1 s, and the body has to shake obviously. Moreover, Fig. 8(c) and (d) show the influence of the interaction between the onboard manipulator and the vehicle on the manipulator, which is represented by the drive torque of the manipulator (taking the second joint as an example) and the rolling angle of its body (manipulator fixed). We can see that the vehicle accelerates starting at time 0 s, its joint peak driving torque and body roll angle all increase.

In the second experiment, the calculated TOM, TOM transfer, and the measured body roll angle under the three schemes are shown in Fig. 9(a)-(h). The moving onboard manipulator was adjusted to the optimal steady state before recording, and the current body roll angle was set to be 0°. Also, the triggered and deactivated margins for tip-over prediction algorithm are set as $TOM_2 = -500$ Nm, $TOM_1 = -10$ Nm.

The TOM calculation results under three schemes are shown in Fig. 9(a), (c) and (e), respectively. The TOM on the TOA_{12} and TOA_{24} gradually reduced, while the TOM on the TOA_{31} and TOA_{43} is gradually increased, which reflected the tipping stability of the robot directly. The TOM on the four tilting axes tends to be zero, and the moving onboard manipulator tends to be stable. The calculation results of TOM transfer under the three schemes are shown in Fig. 9(b), (d) and (f). The values of ΔTOA_{12}, ΔTOA_{24}, ΔTOA_{43}, and ΔTOA_{31} of the four TOM transfer quantities

tend to be zero. From Fig. 9(g), we can see that $\sqrt{\sigma}$ is 14.29 in scheme 1, decay to 9.19 within 0.6 s in scheme 2 and decay to 6.86 within 0.6 s in scheme 3. $\sqrt{\sigma}$ represents the proximity of the current state of the mobile manipulator to the optimal steady state, the smaller the value, the more stable the system, and the recorded body roll angles under the three schemes are as shown in Fig. 9(h). In scheme 1, the rolling angle fluctuates around $-0.04°$. In scheme 2, the rolling angle reversely changes to $-0.066°$ at 0.22 s and then rises to 0 within 0.6 s. In scheme 3, the rolling angle reversely changes to -0.081 at 0.18 s and then rises to 0 within 0.54 s. The short-term instability phenomenon of schemes 2 and 3 is caused by the sudden change of acceleration in the high-velocity movement of the mobile manipulator, so it is not apparent at low velocity. In general, since the mobile platform's inertia of the mobile manipulator is much larger than the onboard manipulator, this transient instability phenomenon has little effect on the stability of the robot. So the tip-over prediction algorithm and the real-time prevention algorithm proposed in this paper are effective, and the tipping-over stability of the robot is significantly improved. Besides, when the ground angle θ_m is non-zero, the algorithm is also applicable to wheeled robots negotiating slopes.

VI. CONCLUSION AND FUTURE WORK

The force interaction between wheel-terrain and vehicle-manipulator has been analyzed by kinematics and force analysis of mobile manipulator, and an ITOMSC for a wheeled mobile manipulator is presented. Newton-Euler method is employed to calculate the reaction force and moment where the onboard manipulator exerted on the vehicle, and vehicle dynamics is used to calculate the reaction force and moment where the ground acted on the vehicle. Tip-over stability criteria are derived by judging the TOM calculated at the different TOA. Comparing with FA, MHS, the criterion is sensitive to the TOM, better timeliness (in Table 2) and suitable for wheeled robot systems that are running on any terrain and subjected to centrifugal force, inertial force and other external forces. Moreover, based on the minimum TOM transfer, a real-time tip-over avoidance algorithm is proposed by adjusting the pose of the onboard manipulator or changing the velocity of the vehicle. The proposed algorithm is simulated and analyzed in MATLAB software, and it is also verified by some experiments on a four-wheel manipulator robot. Simulation and experimental results indicate this proposed algorithm can be used for tip-over predication and avoidance of a wheeled mobile manipulator under a flat road even a slope. And in future work, it's expected this algorithm will also be able to employed in the legged mobile robot.

NOMENCLATURES

L	The length of the wheeled mobile platform
d_m	The width of the wheeled mobile platform
R	The wheel radius of the wheeled mobile platform
m_m	The total mass of the wheeled mobile platform includes the onboard manipulator controller
m_r	The total mass of the onboard manipulator
m_i	The onboard manipulator i-th joint mass, $i = 1 - 6$
ϕ_M	The rotation angle of the mobile platform in the z-direction
θ_m	The incline angle of the ground
l_i	The length of the onboard manipulator i-th link, $i = 1 - 6$
ω_j	The velocity of vehicle j-th wheel, $j = 1 - 4$
α	The included angle between the line connecting the origin O_R and the origin O_M in the x-direction
β	The angle between the roller shaft and body shaft
$\boldsymbol{J}_m$	Jacobi matrix of the mobile platform, $\boldsymbol{J}_m \in R^{3\times4}$
$\boldsymbol{J}_r$	Jacobi matrix of the onboard manipulator, $\boldsymbol{J}_r \in R^{6\times6}$
$\boldsymbol{J}$	Jacobi matrix of the mobile manipulator, $\boldsymbol{J}_r \in R^{6\times10}$
F_{fx}, F_{fy}	Rolling resistance in the x direction and y direction
F_{wx}, F_{wy}	The WMM air resistance in the x-direction and y direction
F_i	The WMM horizontal component of gravity
F_{ax}, F_{ay}	The WMM acceleration resistance in the x-direction and y-direction
μ_x, μ_y	The coefficient of x-direction and y-direction rolling friction
α_i	The angle between the $\hat{Z}_i$ and the $\hat{Z}_{i+1}$ axes measured in the right-hand sense about $\hat{X}_i$
a_i	The distance between the $\hat{Z}_i$ and the $\hat{Z}_{i+1}$ axes, measured along $\hat{X}_i$
θ_{i+1}	The angle between the $\hat{X}_i$ and the $\hat{X}_{i+1}$ axes, measured in the right-hand sense about $\hat{Z}_{i+1}$
d_{i+1}	The distance between the $\hat{X}_i$ and the $\hat{X}_{i+1}$ axes, measured along $\hat{Z}_{i+1}$
${}^i_i\dot{\boldsymbol{v}}$	The linear acceleration of i-link of the manipulator with respect to the frame$i$
${}^i_i\dot{\boldsymbol{v}}_c$	The linear acceleration of i-link of the manipulator at COF with respect to the frame$i$
${}^{i+1}_i\boldsymbol{R}$	The rotation matrix of i-link of the manipulator with respect to the frame $i+1$
${}^{i+1}_{i+1}Z$	The rotating shaft of the mobile manipulator joint $i+1$
${}^w\boldsymbol{r}_r$	The position of the end of the mobile manipulator with respect to the frame $O_W X_W Y_W Z_W$
${}^w\dot{\boldsymbol{r}}_{end}$	End velocity of the onboard manipulator with respect to frame $O_W X_W Y_W Z_W$
${}^{tip}\boldsymbol{f}$	External force exert on end of the onboard manipulator

${}^{tip}\boldsymbol{n}$	External torque exert on end of the onboard manipulator
b_0	The y-direction offset of the ICR with respect to $O_R X_R Y_R Z_R$
d_0	The x-direction offset of the ICR with respect to $O_R X_R Y_R Z_R$
$\boldsymbol{M_i}$	The generalized mass matrix of the link i of the onboard manipulator
$\boldsymbol{H_i}$	The cross-term matrix of the link i of the onboard manipulator including centripetal force and gyro torque
$\boldsymbol{X_i}$	The linear acceleration and angular acceleration vectors of the link i of the onboard manipulator
${}^{i}_{i}\boldsymbol{p_c}$	The position vector of the link's COM of the onboard manipulator
${}^{i}_{i}\boldsymbol{I_c}$	The inertia tensor of the link$I$of the onboard manipulator
${}^{i}\boldsymbol{w}_1$	The force and torque caused by the onboard manipulator 's gravity, angular acceleration
${}^{v}\boldsymbol{w}_1$	The constraint force and torque caused by the onboard manipulator 's angular velocity
${}^{cf}\boldsymbol{w}_1$	The constraint force and torque caused by the environment.
$\boldsymbol{M}_R$	The torques where the onboard manipulator exerted on the mobile platform
$\boldsymbol{F}_R$	The forces where the onboard manipulator exerted on the mobile platform
$\boldsymbol{M}_M$	The torques of wheel-train interaction on the mobile platform
$\boldsymbol{G}_M$	The mobile platform gravity
$\boldsymbol{G}_R$	The onboard manipulator gravity
${}^{1}F_{x,y,z}$	The component of the constraint force act on the 1-th joint of the onboard manipulator in x, y and $z$directions
${}^{1}M_{x,y,z}$	The component of the constraint torque act on the 1-th joint of the onboard manipulator in x, y and $z$directions
$\boldsymbol{TOM_{\ddot{u}C1}}$	The TOM on the TOA $\boldsymbol{o}_{ii+1}$
$\boldsymbol{TOM_{opt}}$	TOM value under a optimal configuration
$TOM_{\max}$	The maximum TOM sustained on the TOA
TOM_1	The upper limit of TOM's work
TOM_2	The lower limit of TOM's work
σ	Optimization function for avoiding tipping
$\dot{q}_i$	The angular velocity of the onboard manipulator joint$i$-th
$\ddot{q}_i$	The angular accelation of the onboard manipulator joint$i$-th
$\dot{\boldsymbol{\xi}}$	The motion velocity of the wheeled mobile platform
${}^{m}\dot{x}_m$	The x-direction velocity of the wheeled mobile platform in the frame $X_M O_M Y_M$
${}^{m}\dot{y}_m$	The y-direction velocity of the wheeled mobile platform in the frame $X_M O_M Y_M$
${}^{m}\dot{\phi}_m$	The rotation velocity of the wheeled mobile platform in the frame $X_M O_M Y_M$
k_i	The weight coefficient of the onboard manipulator joint$i$-th
k_m	The weight coefficient of the mobile platform
k_{mx}	The weight coefficient of the x-direction motion of the mobile platform
k_{my}	The weight coefficient of the y-direction motion of the mobile platform
k_{mz}	The weight coefficient of the$z$-direction rotation of the mobile platform
N_t	The total number of TOM sampling points
n	The number of support polygon vertices
N	The number of DOF of the onboard manipulator
TOA_{ij}	The TOA formed by wheel i and wheel j
$\sigma\ (t_i)$	The optimization function at the time instant t_i

REFERENCES

[1] T. Jung, J. Lim, H. Bae, K. K. Lee, H.-M. Joe, and J.-H. Oh, "Development of the humanoid disaster response platform DRC-HUBO+," *IEEE Trans. Robot.*, vol. 34, no. 1, pp. 1–17, Feb. 2018.

[2] M. Schwarz *et al.*, "Team NimbRo at MBZIRC 2017: Autonomous valve stem turning using a wrench," *J Field. Robot.*, vol. 36, no. 1, pp. 170–182, Apr. 2018.

[3] P. Shen, X. Zhang, and Y. Fang, "Complete and time-optimal path-constrained trajectory planning with torque and velocity constraints: Theory and applications," *IEEE/ASME Trans. Mechatronics*, vol. 23, no. 2, pp. 735–746, Apr. 2018.

[4] S. Aguilera-Marinovic, M. Torres-Torriti, and F. Auat-Cheein, "General dynamic model for skid-steer mobile manipulators with wheel–ground interactions," *IEEE/ASME Trans. Mechatronics*, vol. 22, no. 1, pp. 433–444, Feb. 2017.

[5] E. Krotkov *et al.*, "The DARPA robotics challenge finals: Results and perspectives," *J Field Robot.*, vol. 34, no. 2, pp. 229–240, Nov. 2017.

[6] M. Vukobratović and B. Borovac, "Zero-moment point–thirty five years of its life," *Int. J. Humanoid Robot.*, vol. , no. 1, pp. 157–173, Jan. 2004.

[7] Q. Huang, S. Sugano, and I. Kato, "Stability control for a mobile manipulator using a potential method," in *Proc. IEEE/RSJ Int. Conf. Intell. Robots Syst. (IROS)*, Munich, Germany, Sep. 1994, pp. 839–846.

[8] T.-H. S. Li, Y.-F. Ho, P.-H. Kuo, Y.-T. Ye, and L.-F. Wu, "Natural walking reference generation based on double-link LIPM gait planning algorithm," *IEEE Access*, vol. 5, pp. 2459–2469, 2017.

[9] M. B. Cheng, W. C. Su, C. C. Tsai, and T. Nguyen, "Intelligent tracking control of a dual-arm wheeled mobile manipulator with dynamic uncertainties," *Int. J. Robust Nonlinear Control*, vol. 23, no. 8, pp. 839–857, Apr. 2013.

[10] S. Caron, Q.-C. Pham, and Y. Nakamura, "ZMP support areas for multi-contact mobility under frictional constraints," *IEEE Trans. Robot.*, vol. 33, no. 1, pp. 67–80, Feb. 2017.

[11] S. Sugano, Q. Huang, and I. Kato, "Stability criteria in controlling mobile robotic systems," in *Proc. IEEE/RSJ Int. Conf. Intell. Robot. Syst. (IROS)*, Yokohama, Japan, Jul. 1993, pp. 832–838.

[12] M. H. Korayem, V. Azimirad, A. Nikoobin, and Z. Boroujeni, "Maximum load-carrying capacity of autonomous mobile manipulator in an environment with obstacle considering tip over stability," *Int. J. Adv. Manuf. Technol.*, vol. 46, nos. 5–8, pp. 811–829, Jun. 2010.

[13] A. Goswami, "Postural stability of biped robots and the foot-rotation indicator (FRI) point," *Int. J. Robot. Res.*, vol. 18, no. 6, pp. 523–533, Jun. 1999.

[14] E. G. Papadopoulos and D. A. Rey, "A new measure of tipover stability margin for mobile manipulators," in *Proc. IEEE Int. Conf. Robot. Automat. (ICRA)*, Minneapolis, MN, USA, Apr. 1996, pp. 3111–3116.

[15] S. A. A. Moosavian and K. Alipour, "On the dynamic tip-over stability of wheeled mobile manipulators," *Int. J. Robot. Automat.*, vol. 22, no. 4, p. 322, Jan. 2007.

[16] K. Alipour and S. A. A. Moosavian, "Postural stability of wheeled mobile manipulators with flexible suspension considering tire friction model," in *Proc. IEEE/ASME Int. Conf. Adv. Intell. Mechatron. (AIM)*, Singapore, Jul. 2009, pp. 764–769.
[17] S. A. A. Moosavian and K. Alipour, "Moment-height tip-over measure for stability analysis of mobile robotic systems," in *Proc. IEEE/RSJ Int. Conf. Robot. Syst.*, Beijing, China, Oct. 2006, pp. 5546–5551.
[18] P. R. Roan, A. Burmeister, A. Rahimi, K. Holz, and D. Hooper, "Real-world validation of three tipover algorithms for mobile robots," in *Proc. IEEE Int. Conf. Robot. Automat. (ICRA)*, Anchorage, AK, USA, May 2010, pp. 4431–4436.
[19] Y. Liu and G. Liu, "Interaction analysis and online tip-over avoidance for a reconfigurable tracked mobile modular manipulator negotiating slopes," *IEEE/ASME Trans. Mechatronics*, vol. 15, no. 4, pp. 623–635, Aug. 2010.
[20] A. Ghasempoor and N. Sepehri, "A measure of machine stability for moving base manipulators," in *Proc. IEEE Int. Conf. Robot. Automat. (ICRA)*, Nagoya, Japan, May 1995, pp. 2249–2254.
[21] S. Guo, T. Song, F. Xi, and R. P. Mohamed, "Tip-over stability analysis for a wheeled mobile manipulator," *J. Dyn. Syst., Meas., Control*, vol. 139, no. 5, Mar. 2017, Art. no. 054501.
[22] S. Ali, A. Moosavian, and K. Alipour, "Stability evaluation of mobile robotic systems using moment-height measure," in *Proc. IEEE Int. Conf. Robot. Automat. Mechatron. (RAM)*, Bangkok, Thailand, Jun. 2006, pp. 1–6.
[23] D. A. Rey and E. G. Papadoupoulos, "Online automatic tipover prevention for mobile manipulators," in *Proc. IEEE/RSJ Int. Conf. Intell. Robot. Syst. (IROS)*, Grenoble, France, Sep. 1997, pp. 1273–1278.
[24] Y. Liu and Y. Liu, "Real-time tip-over prevention and path following control for redundant nonholonomic mobile modular manipulators via fuzzy and neural-fuzzy approaches," *J. Dyn. Syst., Meas., Control*, vol. 128, no. 4, pp. 753–764, Dec. 2006.
[25] K. Alipour, A. Hasanpour, and P. Daemy, "Comparing two online tip-over avoidance algorithms for mobile manipulators," in *Proc. 2nd RSI/ISM Int. Conf. Robot. Mechatron. (ICRoM)*, Tehran, Iran, Oct. 2014, pp. 310–315.
[26] T. L. González-Fernández and A. J. Bravo-Valero, "Minimal distance vector. A new approach to avoid tip-over on mobile manipulators," *Iteckne*, vol. 13, no. 1, pp. 7–16, Jun. 2016.
[27] L. Kelley, K. Talke, P. Longhini, and G. Catron, "Tip-over prevention: Adaptive control development and experimentation," in *Proc. IEEE Int. Conf. Robot. Automat. (ICRA)*, Seattle, WA, USA, May 2015, pp. 4367–4372.
[28] M. J. A. Safar, K. Watanabe, S. Maeyama, and I. Nagai, "Tip-over prevention for a holonomic omnidirectional mobile robot with ADWCs using SGCMG," in *Proc. IEEE Int. Conf. Mechatron. Automat. (ICMA)*, Takamatsu, Japan, Aug. 2013, pp. 704–709.
[29] A. Meghdari, D. Naderi, and S. Eslami, "Optimal stability of a redundant mobile manipulator via genetic algorithm," *Robotica*, vol. 24, no. 6, pp. 739–743, Nov. 2006.
[30] R. Rajamani, "Longitudinal vehicle dynamics," in *Vehicle Dynamics and Control*, 2nd ed. New York, NY, USA: Springer, 2006, pp. 87–111.
[31] C. G. Lo Bianco, "Evaluation of generalized force derivatives by means of a recursive Newton–euler approach," *IEEE Trans. Robot.*, vol. 25, no. 4, pp. 954–959, Aug. 2009.
[32] T. Song, F. Xi, S. Guo, and Y. Lin, "Optimization of a mobile platform for a wheeled manipulator," *J. Mech. Robot.*, vol. 8, no. 6, Dec. 2016, Art. no. 061007.

XIAOJUN DING received the B.S. and M.S. degrees (Hons.) in mechanical engineering from Ningxia University, China, in 2010 and 2013, respectively. He is currently pursuing the Ph.D. degree in mechanical engineering with the State Key Laboratory of Digital Manufacturing Equipment and Technology, Huazhong University of Science and Technology, China. His research interests include dynamics modeling, automatic control, motion/path planning of robotic systems, and tip-over stability analysis of mobile robots.

YI LIU received the Diploma degree in electronic information engineering from the China University of Geosciences, the master's degree in control theory and control engineering from the Hubei University of Technology, and the Ph.D. degree in system analysis and integration from the Huazhong University of Science and Technology, where he is currently an Associate Professor with the School of Hydropower and Information Engineering. His research interests include intelligent electromechanical systems, artificial intelligence, and system modeling.

JIN HOU received the B.S. degree (Hons.) in mechanical engineering from Southwest Jiaotong University, China, in 2017. He is currently pursuing the M.S. degree in mechanical engineering with the State Key Laboratory of Digital Manufacturing Equipment and Technology, Huazhong University of Science and Technology, China. His research interests include soft and hard framework design of robot, motion/path planning of robotic systems, and tip-over stability analysis of mobile robots.

QIN MA received the B.S. degree from the Lanzhou University of Technology, in 2017. She is currently pursuing the master's degree with the Water Conservancy Project, Huazhong University of Science and Technology, China. Her research interests include the intelligent electromechanical systems, hydrological forecast, and system modeling.